Investigations on stability and control characteristics of a CS-VLA certified aircraft using wind tunnel test data

Article *in* Proceedings of the Institution of Mechanical Engineers Part G Journal of Aerospace Engineering · February 2016

DOI: 10.1177/0954410016632016

CITATIONS
7

READS
6,337

4 authors:

Nhu Van Nguyen
Viettel Aerospace Institute-VTX
113 PUBLICATIONS **419** CITATIONS
SEE PROFILE

Maxim Tyan
Konkuk University
121 PUBLICATIONS **287** CITATIONS
SEE PROFILE

Jae-Woo Lee
Konkuk University
1,211 PUBLICATIONS **17,237** CITATIONS
SEE PROFILE

Sang-Ho Kim
Konkuk University
11 PUBLICATIONS **52** CITATIONS
SEE PROFILE

Original Article

Institution of MECHANICAL ENGINEERS
Journal of AEROSPACE ENGINEERING

Proc IMechE Part G:
J Aerospace Engineering
0(0) 1–16

DOI: 10.1177/0954410016632016
uk.sagepub.com/jaero
SAGE

Investigations on stability and control characteristics of a CS-VLA certified aircraft using wind tunnel test data

Nhu Van Nguyen, Maxim Tyan, Jae-Woo Lee and Sangho Kim

Abstract

The stability and control characteristics using a wind tunnel test data process are proposed and developed to investigate the stability and control characteristics of a CS-VLA certified aircraft and to comply with the CS-VLA subpart B at the preliminary design review (PDR) and critical design review (CDR) stage. The aerodynamic characteristics of a 20% scale model are provided and investigated with clean, rudder, aileron, elevator, and winglet effects. The Mach and Reynolds correction methods are proposed to correct the aerodynamics of the scale model for stability and control analysis to obtain more reliable and accurate results of the full-scale model. The aerodynamic inputs and moment of inertia (MOI) comparison between the PDR and CDR stage show good agreement in the trends of stability and control derivatives. The CDR analysis results with the corrected wind tunnel test data and accurate MOI are investigated with respect to the longitudinal and lateral stability, control, and handling qualities to comply with the CS-VLA 173, CS-VLA 177, and CS-VLA 181 for finalizing the configuration in the CDR stage.

Keywords

Wind tunnel data, stability and control, CS-VLA aircraft, flying qualities, CS-VLA subpart B

Date received: 28 August 2015; accepted: 11 January 2016

Introduction

The growth in the general aviation industry has recently been very fast. In 2007, a massive impact on the general aviation manufacturing industry occurred when the number of produced aircrafts reached 4276. The number of produced aircrafts, reported in 2013, still reached 2353 aircrafts, with global revenue of US$23.45 billion even in the poor economic environment.[1] The industry leader in general aviation is CESSNA Aircraft Co., USA. In addition to that, there are many light aircraft makers in the world, such as Bombardier-Canada, Embraer-Brazil, Flight Design GmbH-Germany, and Tecnam-Italy.[1] Similarly, the Korean Government boosted the light aircraft development program in 2010.[2] The aircraft design development process includes system requirements review (SRR), system design review (SDR), preliminary design review (PDR), and critical design review (CDR). At each different level of the design stage, various fidelity analysis solvers are used to support the decision-making when changing aircraft configurations. The main aircraft configuration is nearly set after the CDR stage, in which wind tunnel data on a scale test model is extensively used for performance, stability & control (S&C), and structure analysis to comply with subpart B and C regulations to apply for aircraft certification.

A flight test must be performed for the aircraft certification application to verify the previous design stage performance and stability characteristics.[3] The twin-engine light aircraft P2006T flight test data are used to demonstrate aircraft safety and obtain CS-23 or FAR23 certification.[3] However, it is very important to conduct accurate stability and control estimation at the CDR stage before moving to a flight test. Several studies on stability and control are conducted by using the wind tunnel data and computational fluid dynamics (CFD) to enhance the stability and control analysis results. *Kasim Biber* presented the stability and control characteristics of a new FAR23 airplane using a power-off and stick-fixed 1/12 scale model for static stability and open-loop dynamic stability and response.[4] Nicolosi et al.[5] obtained the stability derivatives from the output error method (OEM), which is a known identification technique for P2006T twin-engine aircraft. Some of the stability

Department of Aerospace Information Engineering, Konkuk University, Seoul, South Korea

Corresponding author:
Sangho Kim, Department of Aerospace Information Engineering, Konkuk University, 120 Neungdong-ro, Gwangjin-gu, Seoul, Republic of Korea.
Email: kimsh85@konkuk.ac.kr

derivatives obtained from the level flight test and scale wind tunnel test model with correction were used to estimate and assess the flight qualities and longitudinal parameters.

The assessment of stability and performance using flight test data and wind tunnel test data were used for certification of CS-23 or FAR 23. Cummings and Schütte[6] introduced the integrated computational/experimental approach to predict UCAV static and dynamic stability and control. Anton et al.[7] proposed the FDerivatives code with Digital DATCOM and wind tunnel test data to predict delta-wing X-31 aircraft longitudinal dynamic stability, including the short Phugoid mode responses. The wind tunnel test data were used and validated for the proposed method. Lee and Yoon[8] presented a method to estimate the lateral-directional flight parameters of a light airplane from the flight test data and simulated responses. Moreover, the Reynolds and Mach number correction are issues that must be handled for the stability and control characteristic estimation of a full-scale model. The main challenges are the extrapolation from the scale model to free flight conditions, in which the model support, wall interference, aero-elastic effects, and potentially lower Reynolds number in the wind tunnel must be corrected.[9] Pettersson and Rizzi[9] presented the modern approaches, in which CFD is used to extrapolate the data from a wind tunnel test accurately and appropriately.

Many studies have focused on the free flight data extrapolation from scale wind tunnel data for the assessment of aircraft performance and S&C with more accurate and reliable approaches. Traub[10] proposed a method for the lift and drag extrapolation from wind tunnel test data with simplified assumptions. The extrapolation results showed encouraging agreement when compared to the wind tunnel test data. Thamarai Selvi et al.[11] introduced the interpolation and extrapolation of wind tunnel test data using a neural network for the free flight condition. The Reynolds number effects on off-design stability and control characteristics were investigated with respect to supersonic transport at departure and landing flight conditions, which were used for the supersonic transport operation.[12]

In this study, the stability and control characteristics of light aircraft using wind tunnel test data are investigated for the assessment of flying qualities and static and dynamic stability, which are compliant with the CS-VLA regulations and design requirements at the CDR stage. The newly designed light aircraft—20% scale model with wing-cuff, winglet, and low wing—for high maneuvering performance are tested using a wind tunnel test with variations of angle of attack (AoA), angle of sideslip (AoS), flap, rudder, elevator, and aileron deflection. The 20% scale wind tunnel test data are provided under normal flight conditions for the assessment of flying qualities, stability and control. The stability and control derivatives and flying qualities are investigated and compared to the analysis results at the PDR stage. The Reynolds and speed correction methods are provided to process the raw wind tunnel test data from the scale model to provide more reliable and accurate stability and control characteristics of light aircraft.

Stability and control characteristics using wind tunnel test data process

The stability and control characteristics using the wind tunnel test data process are presented in Figure 1. It includes the input data, stability and control analysis solver, output data, and CS-VLA: subpart B modules, which cover the investigations of static and dynamic stability and control characteristics and analysis results that are compliant with the airworthiness CS-VLA: subpart B regulations. The reliability analysis results depend on the design stage, in which the fidelity of input data includes the configuration data, aero database (DB), and weight DB, which come from different sources. The design stage goes further, from the conceptual design stage to the preliminary design stage; thus, the reliability of input data has to provide higher accuracy analysis or wind tunnel results to help in fixing the configuration at a later design stage review. The proposed process is to evaluate and investigate the stability and control characteristics at the critical design review (CDR) stage, using the wind tunnel test data to enhance the analysis results to comply with the airworthiness regulation CS-VLA subpart B. Moreover, the proposed process includes the preliminary design review (PDR) stability and control input and analysis results to enhance the PDR analysis tools and analysis results.

Input Data includes the PDR and CDR-input data, as shown in Figure 1, in which the configuration, aero DB, and weight DB are required by the stability and control analysis solver. The panel method AVL,[13] in-house drag code AERO09,[14] and Aircraft DATCOM[15] are used to provide the aerodynamic characteristics at the PDR design stage. The in-house weight analysis is used to estimate the weight components, CG location, MOI, and CG envelope for the S&C analysis solver, as shown in the Input Data block (Figure 1). At the CDR stage, the enhanced multi-fidelity aero-DB using the wind tunnel test data and the detailed mass breakdown report are used to improve the accuracy and reliability of the stability and control analysis results shown in the Input Data block. The enhanced multi-fidelity DB uses the raw wind tunnel test data from the scale model and limited speed test cases to correct the Reynolds and Mach numbers for the full-scale model in an entire flight envelope with the help of variable fidelity analysis and interpolation subroutines, as shown in Figure 1. A high accuracy and fully processed aerodynamics database is obtained

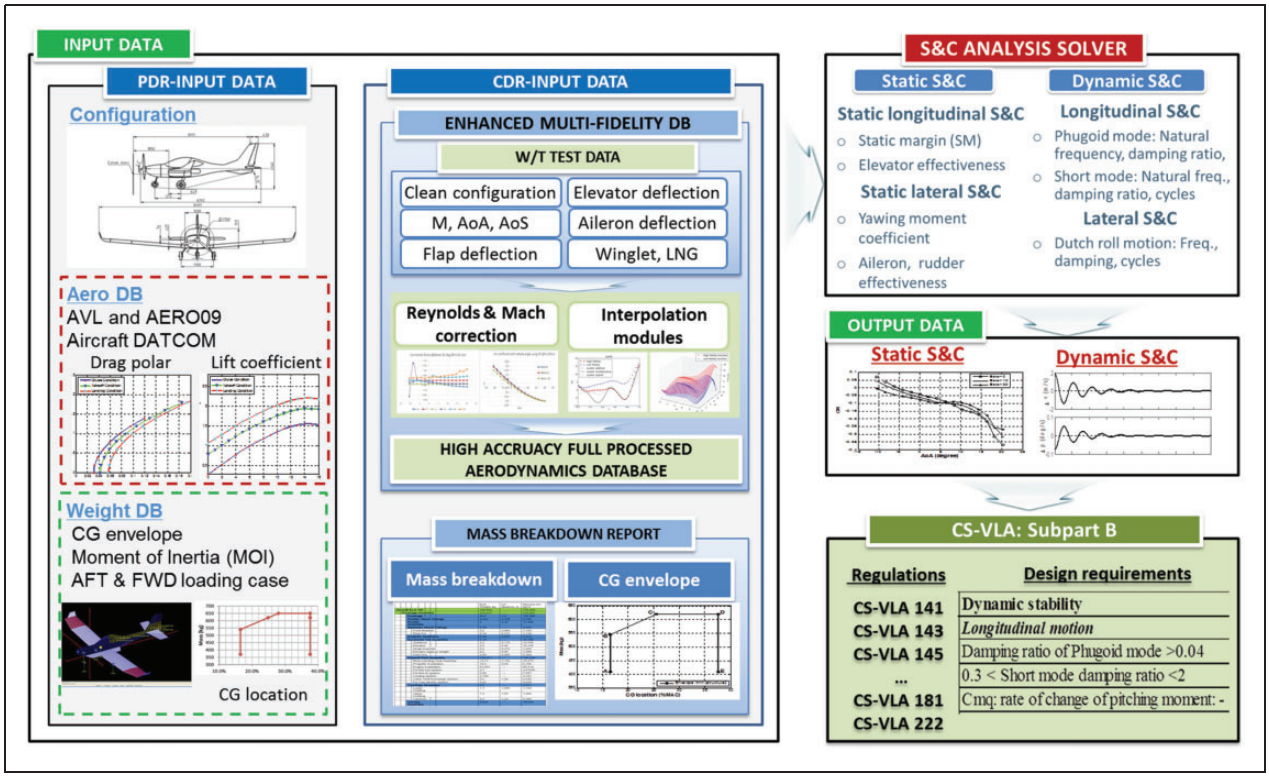

Figure 1. Stability and control characteristics using wind tunnel test data process.

for the S&C analysis solver. Moreover, the mass breakdown report is used to provide the CG envelope and moment of inertia (MOI) calculation more accurately and reliably for S&C dynamic analysis.

S&C Analysis Solver is an in-house code developed for analyzing the variable fidelity of input sources in both the aerodynamic and weight database formats. It has been developed and validated for light aircraft design application,[14] subsonic UAV robust design optimization,[16] and subsonic electric-powered UAV design application.[17] The solver includes the static and dynamic S&C analysis to resolve the governing equation of the longitudinal and lateral motions. The stick force per knots and per "g", as well as the spin recovery analysis, are also included in the S&C analysis solver.[18]

Output Data includes the static and dynamic S&C analysis results, such as static margin (SM), static longitudinal stability, static lateral stability derivatives, and handling qualities for short mode, Phugoid, Spiral, and Dutch-roll motion, as shown in Figure 1.

CS-VLA: subpart B includes the regulation and design requirements for the stability and control analysis evaluation. The stability and control analysis results are used to comply with the regulations and design requirements at this stage.

Wind tunnel test procedure and results

The subsonic wind tunnel test is used from the Republic of Korea Air Force (ROKAF) academy.[19] The close-circuit type wind tunnel test is used. The test section dimensions are 2.45 m-high, 3.5 m-wide, and 8.7 m long. The boundary layer removal system is aimed to simulate the air-flow close to the real aircraft flight condition. The wind tunnel test reaches a maximum speed of 92 m/s with a speed maximum variation of 0.03 m/s with the model scale of 7.26:1. The speed steadiness is less than 0.11% of the average flow. Hence, the stable flow is able to maintain during the experiment. The maximum variations in AoA and AoS are less than 0.1°. The pressure and temperature distributions of the cross-sectional area show a maximum error of 0.5%.[19] The maximum turbulence level at 74 m/s is 0.1%.

Wind tunnel model and test condition

The full scale of the light aircraft is shown in Figure 2. It is a low-wing aircraft with a wing span with winglet of 10.31 m and fuselage length of 6.3 m. The maximum fuselage width and height are 1.28 m and 1.158 m, respectively, to provide the pilot with comfortable space.[20] The wing airfoil was designed for this low-wing light aircraft with high performance and maneuver characteristics.

The wing uses two airfoils, in which the outer wing airfoil (FD14-142) features a "drooped nose" and is designed to allow for a higher than maximum lift coefficient to improve the stall behavior of the aircraft. The inboard wing up to the aileron makes use of a FD14-144 airfoil section. Both airfoils are derivatives from the proven airfoil C180 used on the CT aircraft series.[21] The horizontal tail uses the inverse

NACA 2412 airfoil. The vertical tail uses the symmetrical NACA 0012.

The light aircraft 20% scale test model is shown in Figure 3. The wing-cuff was fabricated as a designed model to increase the light aircraft's performance, as shown in Figure 3(b). The winglet is also tested to observe the winglet aerodynamic characteristics in the wind tunnel test. A landing gear test is also performed. The balance center point is at 0.35 m on the X-axis and 0 on the Y- and Z-axes. The test model center of gravity (CG) is 0.3804 m. The test condition is presented in Table 1 for the speed, angle of attack, side slip angle, aileron, elevator rudder, flap, landing gear, and winglet condition. The test speed is 40 m/s, corresponding to a Reynolds number of 0.6×10^6.

The test condition is presented in Table 1 with the fixed Mach number. The AoA varies from -10° to 20°, and the AoS sweep is from -2° to 20° with the step of 2°. The fairing, winglet, and landing gear effects are tested. The control surfaces, including flap, left and right aileron, elevator, and rudder, are deflected with AoA and an AoS sweep, as shown in Table 1. The six basic output components are the lift force, drag force, side force, pitching moment, yawing moment, and rolling moment coefficients for each combination to be generated.

The coordinate system of light aircraft is presented in Figure 4(a). The sign convention of axis, pitching, rolling, and yawing moment are denoted as shown in Figure 4(a). The sign convention of sideslip angle is shown in Figure 4(b).

The aerodynamic characteristics measurement errors are presented in Table 2. The analysis condition of measurement errors is the clean configuration and AoA of 4.05°. The cruise speed is at 40 m/s with the 95% reliability of flow.[19]

Experimental results

Longitudinal aerodynamics. The longitudinal aerodynamic characteristics with sideslip angle effects are

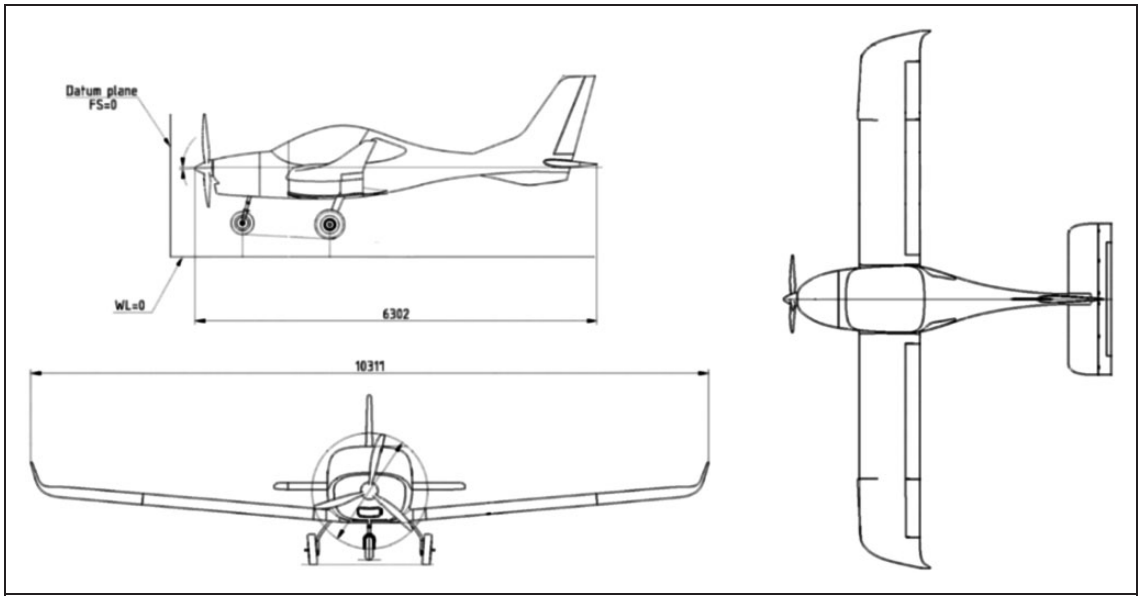

Figure 2. Very light aircraft – 3D view geometry.

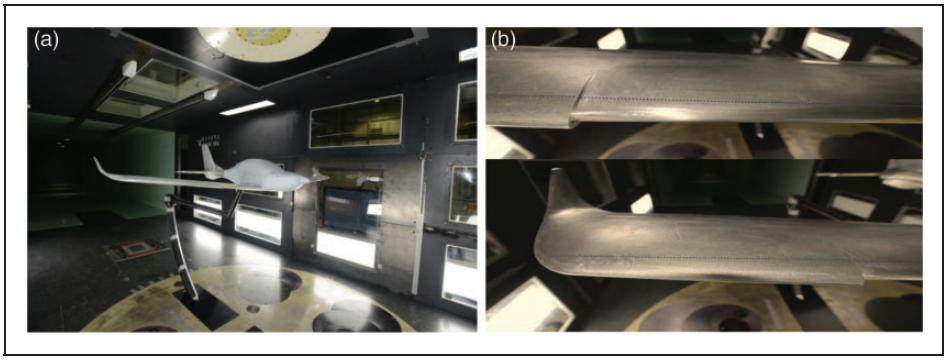

Figure 3. Light aircraft 20% scale test model: (a) 20% scale test model; (b) wing cuff and winglet in different wing sections.

presented in Figure 5. The lift coefficient increases when the AoS increases from 0° to 20° for this light aircraft, as shown in Figure 5(a). A small increment in lift coefficient occurs when the AoS increases due to the low-wing and small dihedral aircraft configuration shown in Figure 2. The sideslip angle affects the lift in the whole range of tested angles of attack as seen in Figure 5(a) and (c). The drag coefficient increases as the AoS increases from 0° to 20° (Figure 5(c)). As a result, the lift-to-drag ratio decreases when the AoS increases (Figure 5(d)). The maximum lift-to-drag ratio reaches approximately 14.2 at an AoA of 5°. This shows a good aerodynamic design of the light aircraft for cruise conditions.

The flap effects on the lift and drag coefficients are obviously presented in Figure 6 for the clean, takeoff, and landing conditions corresponding to flap deflections of 0°, 20°, and 35°. The maximum lift coefficient reaches 1.28, 1.51, and 1.686 for the clean, takeoff, and landing configurations, respectively, as shown in Figure 6(a) for the scale model. The maximum lift coefficient at the landing configuration plays a significant role in complying with the stall speed regulations. The slotted flap design optimization was performed to generate competitive lift characteristics compared to other light aircraft.[22] The stall angles are 15°, 13.5°, and 12.5° for the clean, takeoff, and landing configurations, respectively. The lift coefficient behaviors are also shown to be smooth after the stalling region shown in Figure 6(a). The drag polar for the clean, takeoff, and landing configurations is presented in Figure 6(b).

The elevator effects on the pitching and lift coefficients are investigated in Figure 7(a) and (b) from −25° to 20° of elevator deflection. For the elevator-up, which is negative, the pitching moment coefficient increases to pitch up the nose. The pitching moment coefficient variation shows nonlinear behavior with the elevator deflections in Figure 7(a). The elevator control effectiveness is difficult to predict by using the panel method or empirical relations at the early design stage. The lift coefficient shows the most linear behavior with the elevator deflection in Figure 7(b). For the elevator-down, which is positive, the lift coefficient increases slightly, as shown in Figure 7(b).

Lateral and directional aerodynamics. The effects of the rolling and yawing moment coefficients of lateral and directional aerodynamic characteristics on the sideslip, rudder, and aileron are investigated. The main effects of AoS on the rolling and yawing moments are presented in Figure 8(a) and (b). The rolling moment coefficient becomes more negative when the AoS increases

Table 1. Test condition for 20% VLA scale model.

Item	Value/Range
Flow speed (m/s)	40 m/s ($Re = 6.0 \times 10^5$)
α (deg)	−10°, −8°, −6°, −4°, −2°,
(16 points at β=0°, 10°, 20°)	0°, 2°, 4°, 6°, 8°, 10°, 12°, 14°, 16°, 18°, 20°
β (deg)	−2°, 0°, 2°, 4°, 6°, 8°,
(12 points at α=0°, 10°)	10°, 12°, 14°, 16°, 18°, 20°
Aileron deflection (AL/AR) (deg)	±3°, ±6°, ±9°, ±12°, +17°/−12°, +20°/−12°
Elevator deflection, *E* (deg)	−25°, −17°, −9°, 7°, 14°, 20°
Rudder deflection, *R* (deg)	−9°, −17°, −25°
Flap deflection, *F* (deg)	6°, 20°, 35°
Landing gear	On (Type 1, 2) / Off
Winglet	On/Off

Table 2. Aerodynamic characteristics measurement errors.[19]

	α (deg)	C_L	C_D	C_m
Uncertainty of measurement	±0.05079	±0.0138	±0.00142	±0.00103

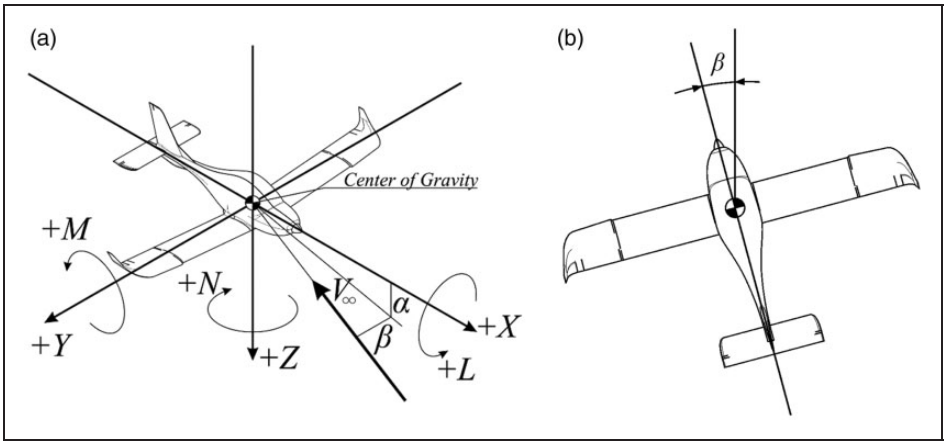

Figure 4. Light aircraft coordinate system and sign convention: (a) light aircraft coordinate system; (b) sideslip side convention.

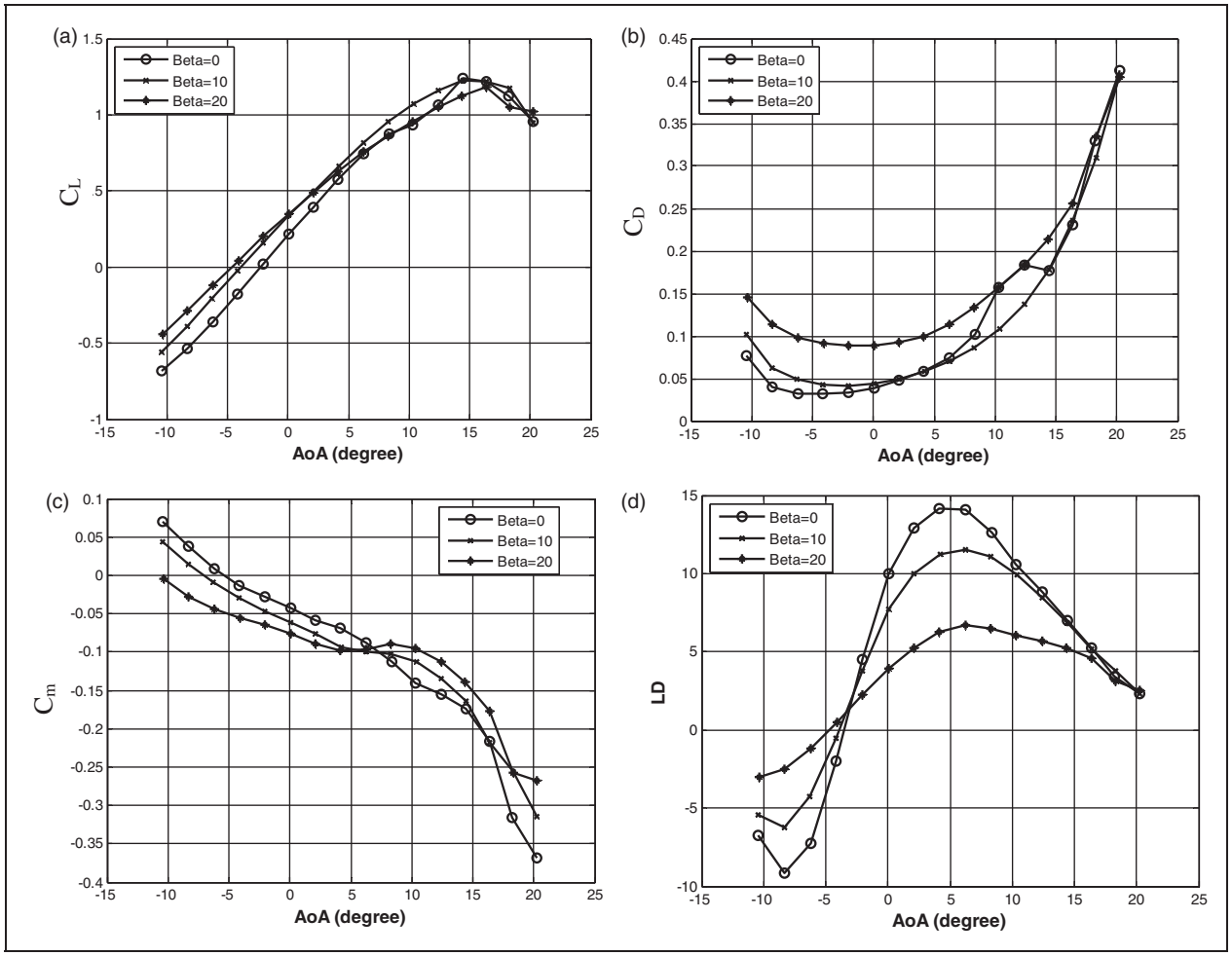

Figure 5. Sideslip angle effects on the longitudinal aerodynamic characteristics: (a) lift coefficient vs AoA at sweep AoS; (b) drag coefficient vs AoA at sweep AoS; (c) pitching moment vs AoA at sweep AoS; (d) lift-drag ratio vs AoA at sweep AoS.

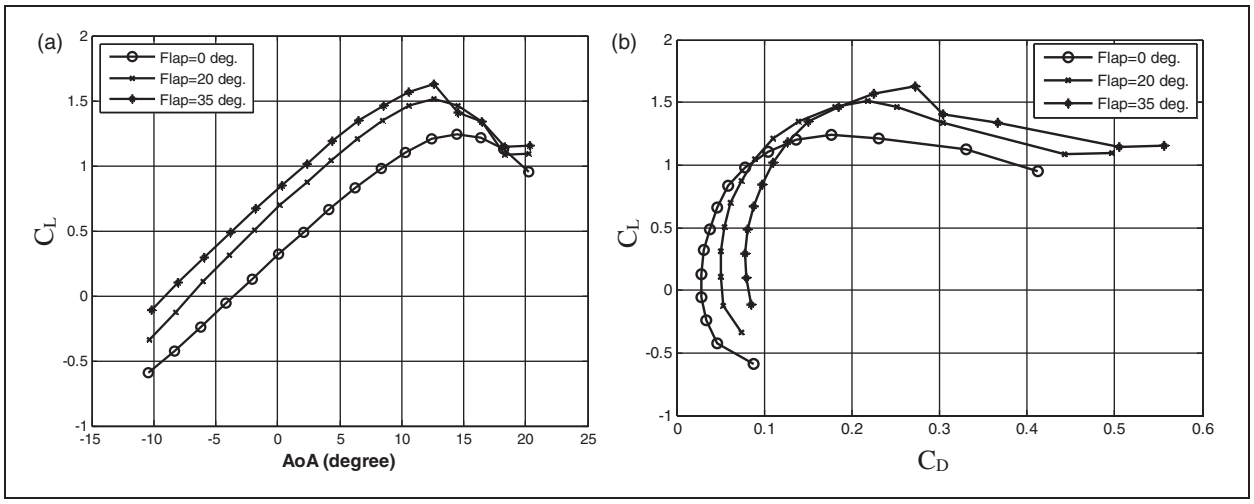

Figure 6. The flap effects on the longitudinal aerodynamic behavior: (a) lift coefficient with flap effects; (b) drag polar with flap effects.

from 0° to 20° in Figure 8(a). The rolling behavior of a low and dihedral wing is shown to be statically stable. The yawing moment coefficient shows an increase when the AoS increases from 0° to 20° in Figure 8(b). This shows the statically lateral stable behavior of the designed aircraft.

The aileron deflection is mainly effected by the rolling moment coefficients, as expected and shown

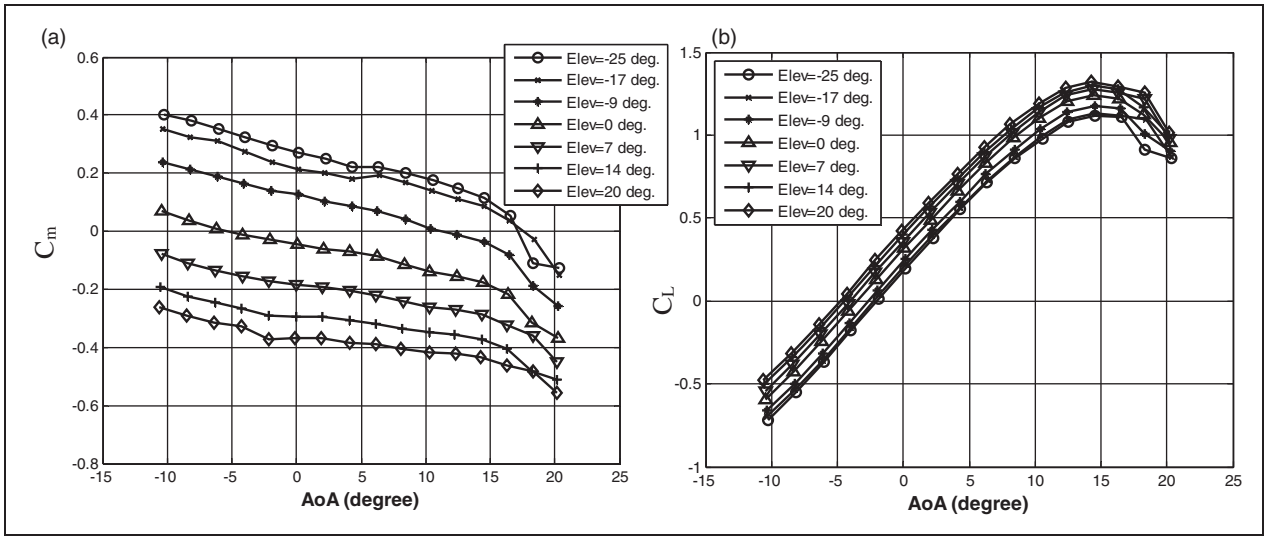

Figure 7. The elevator effects on the longitudinal aerodynamic behavior: (a) pitching moment coefficient with elevator effects; (b) lift coefficient with elevator effects.

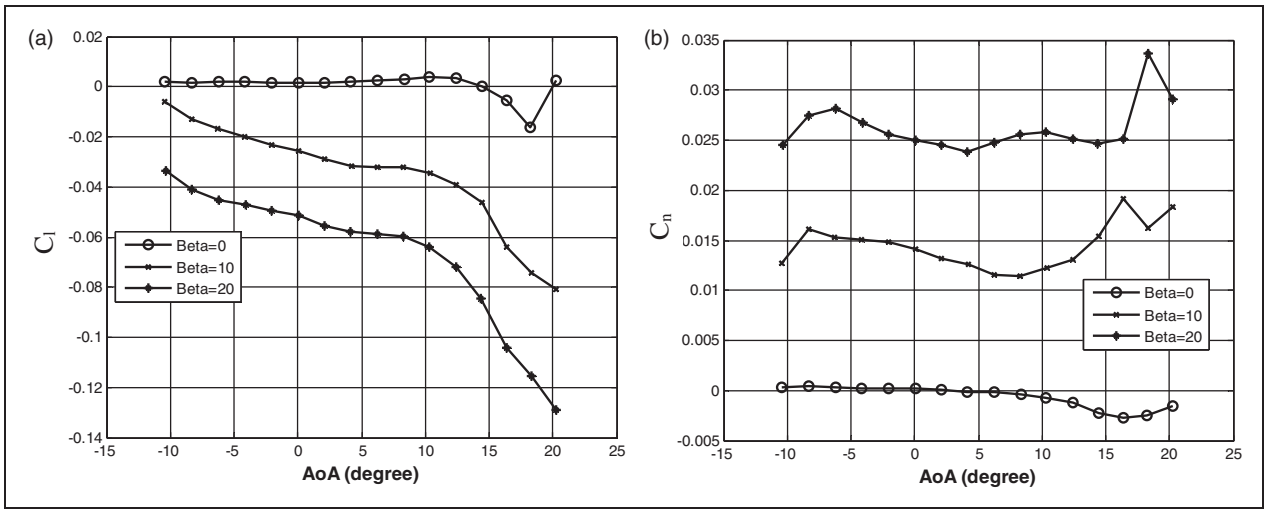

Figure 8. Sideslip angle effects on lateral aerodynamic behavior: (a) rolling moment coefficient with AoS effects; (b) yawing moment coefficient with AoS effects.

in Figure 9(a) for an aileron deflection angle from 0° to 20°. The rolling moment coefficient increases nonlinearly as the aileron deflection angle increases. The aileron control effectiveness shows a small increase when the aileron deflection approximately reaches the maximum deflection angle, as shown in Figure 9(a). The yawing moment coefficient has a small effect when the aileron is deflected, as shown in Figure 9(b). As the aileron deflection angle increases, the yawing moment behavior reduces the directional static stability, which makes the yawing moment coefficient more negative when the aileron deflects.

The rudder deflection is mainly effected by the yawing moments, as shown in Figure 10(a) for a rudder deflection from 0° to −25°. The yawing moment coefficient increases nonlinearly with the rudder deflection. The yawing moment coefficient increases slightly at approximately the maximum rudder deflection of 25°. This shows a large increase for the first rudder deflections from 0° to −9°. The effects of rudder deflection on rolling moments are presented in Figure 10(b). The rolling moment coefficient becomes more negative while the rudder deflects, as shown in Figure 10(b).

Winglet effects. The winglet effects on the wind tunnel test data are investigated for the cases with the winglet either on or off. The winglet effects show an increase in lift coefficient in Figure 11(a). Improvement of the lift-to-drag ratio is also observed in Figure 11(b). Thus, winglet-on obviously improves the aerodynamic performance of the designed aircraft.

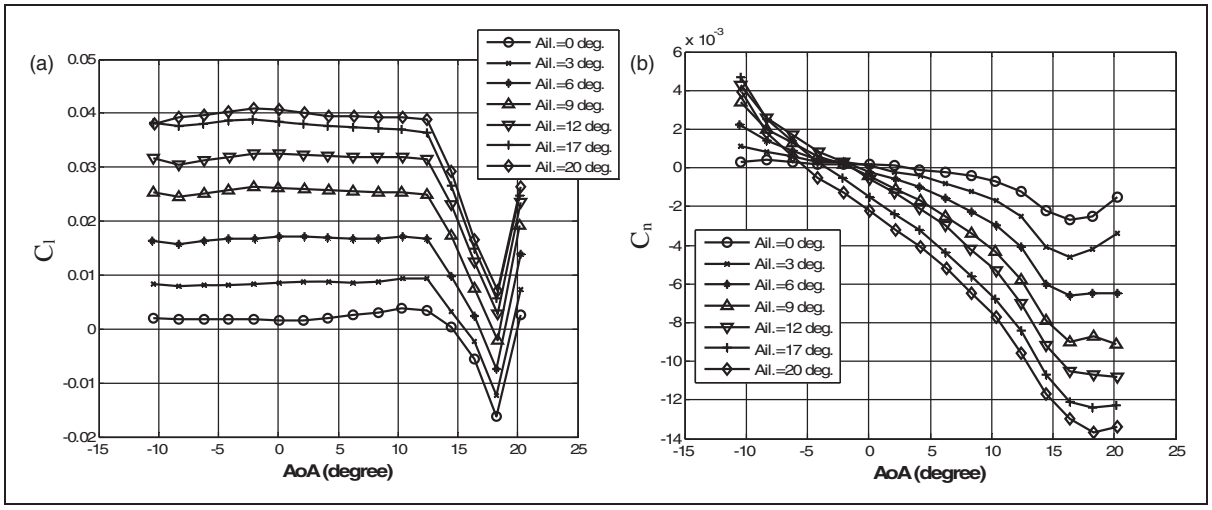

Figure 9. Aileron effects on lateral aerodynamic behavior: (a) rolling moment coefficient with aileron effects; (b) yawing moment coefficient with aileron effects.

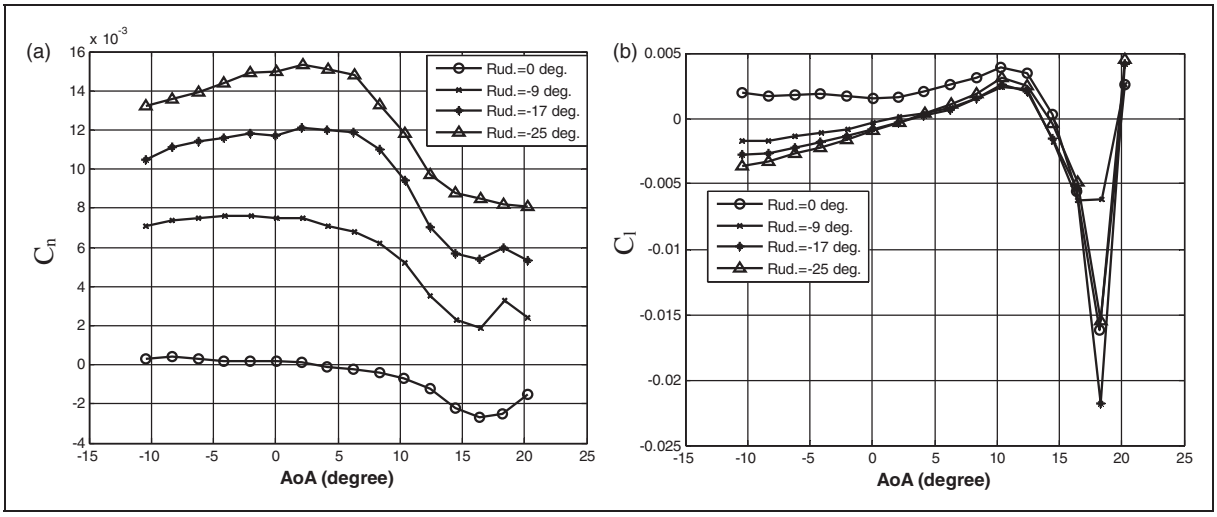

Figure 10. Rudder effects on lateral aerodynamic behavior: (a) yawing moment coefficient with rudder effects; (b) rolling moment coefficient with rudder effects.

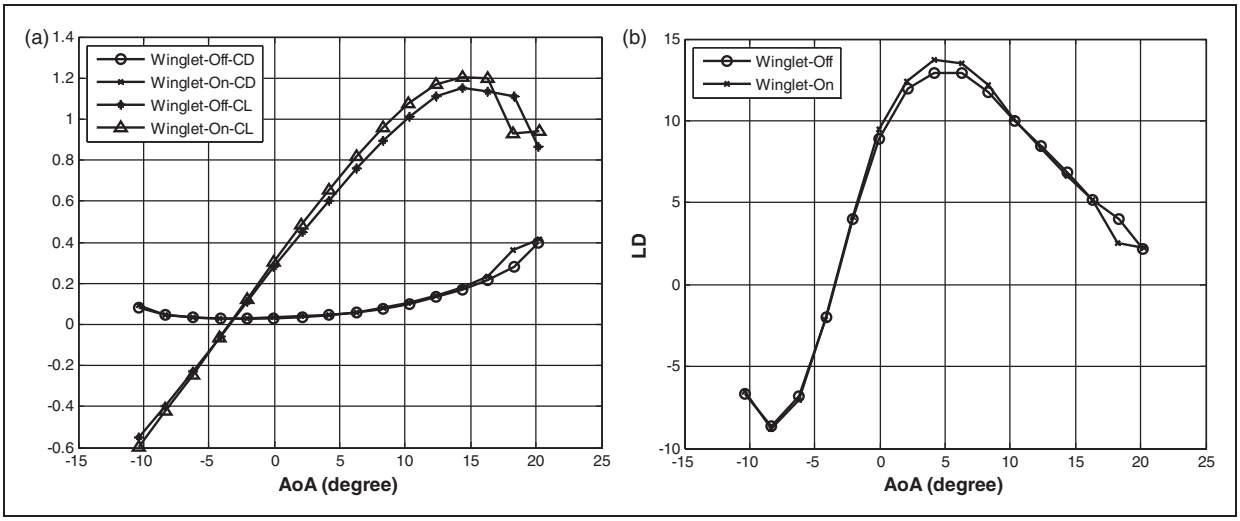

Figure 11. Winglet effects on the aerodynamic characteristics: (a) lift and drag coefficient with winglet effects; (b) lift-over-drag ratio with winglet effects.

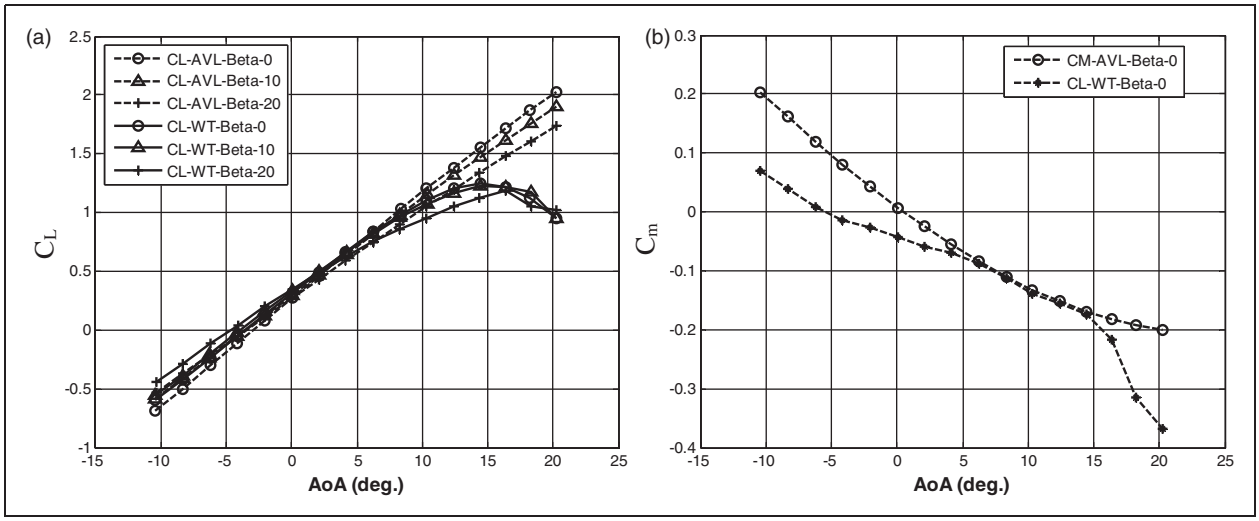

Figure 12. AVL validation results with W/T data for different sideslip angles: (a) lift coefficient comparison with wind tunnel test; (b) pitching moment coefficient comparison.

Reynolds and Mach number correction

Reynolds number correction method. The parasite drag, maximum AoA, and maximum lift coefficient are tested to determine the Reynolds correction effects according to the following equations[23]

$$C_{D_0} = C_{D_0 M@WT} \frac{C_{f\,M@flight}}{C_{f\,M@WT}} \tag{1}$$

where C_f is the skin friction coefficient.

$$C_f = \frac{0.45}{\left(\log_{10} Re\right)^{2.58}\left(1 + 0.144M^2\right)^{0.58}} \tag{2}$$

The maximum lift and maximum AoA are corrected according to the following equations[24]

$$\begin{aligned} \Delta C_{Lmax} &= A \ln\left(\frac{Re_{M@flight}}{Re_{M@WT}}\right) \quad \text{and} \\ \Delta\alpha_{max} &= B \ln\left(\frac{Re_{M@flight}}{Re_{M@WT}}\right) \end{aligned} \tag{3}$$

where A and B are the corrected factors from wind tunnel test data.

Mach number correction method. The Mach number correction for stability and control derivatives is presented as follows[4]

$$\text{Derivative} = \text{Derivative}_{M@WT} \frac{\text{Derivative}_{M@flight}}{\text{Derivative}_{M@WT}} \tag{4}$$

The derivative correction at different Mach numbers is shown in equation (4). $\text{Derivative}_{M@flight}$ and $\text{Derivative}_{M@WT}$ are calculated by using the panel method code AVL.[13] AVL is validated with W/T data at a speed of 40 m/s, as shown in Figure 12.

The center of gravity envelope and analysis condition

The CG envelope of light aircraft is shown in Figure 12. The forward CG is located at 16.5% MAC for points A and B. The aft CG is located at 37.6% MAC for points D and E in Figure 13.[20] Points C and D are 25.5% MAC and the aft CG under the MTOW condition, respectively. The critical loading condition and flight condition are used for stability and control characteristics investigation in the later parts. The design cruise speed condition is 60 m/s. The MTOW is 620 kg, as shown in Figure 13.

Stability and control characteristics

Moment of inertia calculation

$$\begin{aligned} I_{xx} &= I_{xxCG} + m(y_{CG}^2 + z_{CG}^2), \\ I_{yy} &= I_{yyCG} + m(x_{CG}^2 + z_{CG}^2), \\ I_{zz} &= I_{zzCG} + m(x_{CG}^2 + y_{CG}^2) \\ I_{xy} &= I_{xyCG} + m(x_{CG}^2 + y_{CG}^2), \\ I_{xz} &= I_{xzCG} + m(x_{CG}^2 + z_{CG}^2), \\ I_{yz} &= I_{yzCG} + m(y_{CG}^2 + z_{CG}^2) \end{aligned} \tag{5}$$

where I_{xxCG}, I_{yyCG}, I_{zzCG} are moment of inertia of the body about its own CG; x_{CG}, y_{CG}, z_{CG} are distance from the reference point to the CG of the body; M are the mass components.

The MOI is an extremely important value for estimating the dynamic stability and control. Moreover, the MOI is very hard to predict accurately during the conceptual design and preliminary design stage.

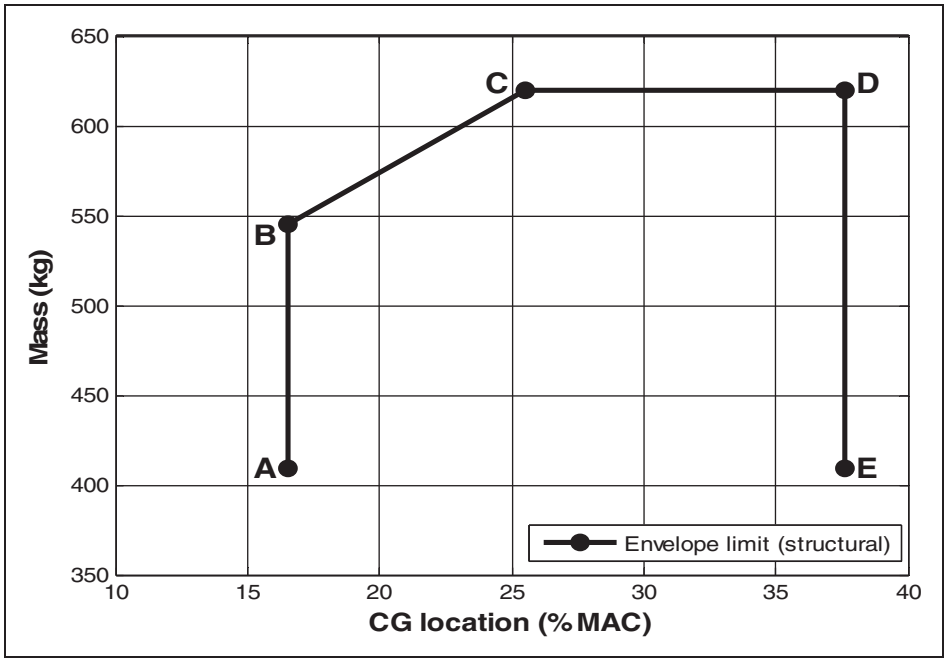

Figure 13. Light aircraft CG envelope.

Table 3. MOI comparison between PDR and CDR stage.

MOI of light aircraft (CDR stage)						
I_{xx}	I_{yy}	I_{zz}	I_{xy}	I_{xz}	I_{yz}	
1.E + 09	1.E + 09	2.E + 09	3.E + 08	1.E + 08	1.E + 08	kg.mm^2
990.98	1262.77	1967.94	288.31	136.99	128.27	kg.m^2
MOI of light aircraft (PDR stage)						
759.24	655.19	1199.07	0	0	0	slug.ft^2
1029.39	888.32	1625.72	0	0	0	kg.m^2

MOI: moment of inertia; CDR: critical design review; PDR: preliminary design review.

Table 4. Longitudinal motion: static characteristic and CS-VLA 173 compliance checking.

Requirements	VLA_CDR	VLA_PDR	Evaluation	Note
$-1.5 < C_{m\alpha}(1/\text{rad}) < -0.3$	−0.414	−0.825	Satisfied	Mid CG
$10\ \% < SM < 30\ \%$	14.31%	17.5%	Satisfied	Mid CG

The MOI is predicted by using the detailed mass breakdown at the CDR stage, in which each mass component, including the wing, fuselage, horizontal and vertical tail, control panel, battery, pilot, and luggage, is calculated by using equation (5).[25] The MOI is composed of its own CG and the total aircraft CG. Therefore, a more accurate and reliable MOI is obtained at the CDR stage compared to the PDR stage, as shown in Table 3.[26]

Longitudinal motions

Static longitudinal characteristics. The static longitudinal characteristics of the light aircraft are presented in Table 4. The statement of certification regulations CS-VLA 173 is listed as requirements for $C_{m\alpha}$ and SM at the mid CG condition.[27,28] The results of the light aircraft at the CDR stage (VLA_CDR) locate in the interval of requirements for CS-VLA 173. The comparison results between VLA_CDR and VLA_PDR are shown in the Table 4. The VLA_PDR results show more stable and conservative results compared to the current VLA_CDR results. VLA_PDR results use the AVL method to estimate the longitudinal static characteristics at the conceptual design stage. Thus, it is expected to lower fidelity and produce more conservative results. The collection of longitudinal static stability coefficient for the general aviation

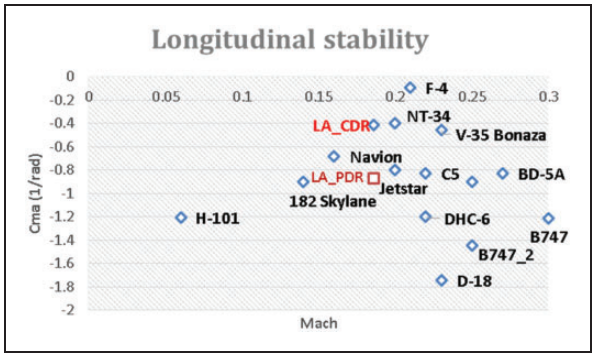

Figure 14. Static longitudinal characteristics of very light aircraft (VLA) comparison.

Table 5. Longitudinal stability and control derivatives comparison.

Derivatives	VLA_CDR (W/T data)	VLA_PDR (AVL data)	Note
C_{Xu}	−0.138	−0.013	1/rad
C_{Zu}	−0.961	−0.339	1/rad
C_{mu}	0	−0.302	1/rad
$C_{X\alpha}$	0.1771	X	1/rad
$C_{Z\alpha}$	−5.19	−5.58	1/rad
$C_{m\alpha}$	−0.5	−2.905	1/rad
$C_{Z\dot{\alpha}}$	−1.669	X	1/rad
$C_{m\dot{\alpha}}$	−5.62	X	1/rad
C_{Zq}	−4.667	X	1/rad
C_{mq}	−15.72	−21.86	1/rad
$C_{Z\delta e}$	−0.3626	0.0086	1/rad
$C_{m\delta e}$	−1.105	−0.031	1/rad

aircraft within the Mach number of 0.05 to 0.3 is obtained to check for the new design light aircraft[25] at the PDR and CDR stage. The mapping $C_{m\alpha}$ results compared to a similar aircraft speed regime for Mach numbers from 0.05 to 0.3 are shown in Figure 14.[25] The designed light aircraft shows light static stability at the mid CG analysis condition. The mapping longitudinal static stability results confirm the normal and safe design configuration of a new light aircraft compared to the existing light aircrafts.

Dynamic longitudinal characteristics. The longitudinal stability and control derivatives for the CDR stage are corrected at cruise speed from the wind tunnel test data, as shown in Table 5. The derivatives are compared to results from AVL analysis, which are denoted as VLA_PDR. The AVL shows the most correct trend for the stability and control derivatives, as shown in Table 5. However, the VLA_PDR results show very poor prediction results for control effectiveness coefficients $C_{Z\delta e}$ and $C_{m\delta e}$. The relatively big differences between the wind tunnel test data and computation method using the panel method (AVL)[13] comes from

Table 6. Longitudinal motion: Dynamic characteristic and CS-VLA 181 compliance checking.

Requirements	VLA_CDR	VLA_PDR	Evaluation	Note
$\xi_{phugoid} \geqslant 0.04$	0.186	0.156	Satisfied	Mid CG
$0.3 \leqslant \xi_{short} \leqslant 2$	0.788	0.710	Satisfied	Mid CG
$-40 \leqslant C_{mq} \leqslant -5$	−15.72	−21.86	Satisfied	Mid CG

the linear aerodynamic prediction code – AVL for the longitudinal control effectiveness prediction $C_{Z\delta e}$ and $C_{m\delta e}$ as shown in Table 5. The panel method AVL has difficulties to predict the nonlinear aerodynamic behaviors such as high AoA conditions and the control surface deflections.[13] The panel method is suitable for the earlier design stage.

Thus, the VLA_CDR dynamic longitudinal motion results are enhanced by using the accurate corrected wind tunnel test data for analyzing the longitudinal motion. Moreover, the comparison between VLA_CDR and VLA_PDR indicates the correct trends of stability and control derivatives at the conceptual design stage compared to the wind tunnel test data model. Therefore, it also enhances the design approach for light aircraft development.

The dynamic longitudinal motion characteristics are derived from the linearized governing equation with small disturbance theory.[29–31] The equation of longitudinal motion is shown as follows

$$x' = Ax + \eta B \tag{6}$$

where $x = [\Delta u, \Delta\alpha, \Delta\theta, \Delta\gamma]$ is the state vector, $\eta = [\Delta\delta_T, \Delta\delta_e]$ is the control vector, and matrices A and B contain the stability and control derivatives, as shown in Table 5. The longitudinal motion and response results are shown in Table 6. The airworthiness regulation for dynamic stability is stated in CS-VLA 181.[28] The handling qualities requirements for the longitudinal motion of this light aircraft with a comfortable level of acceptability are shown in Table 6.[27,32,33] The handling qualities requirements for longitudinal motions are composed of $\xi_{phugoid}$, ξ_{short}, and C_{mq} referred from other studies.[32,33] The results shown in Table 6 are analyzed at the cruise condition and at mid CG. The comparison results are also made for the previous PDR results. The results are compliant with CS-VLA 181.

Moreover, CS-VLA 181 states that short mode must be heavily damped from the stall speed to maximum speed. Therefore, the variations of Phugoid and the short mode damping ratio from the stall speed to maximum speed are shown in Figure 15(a) and (b) for a light aircraft weight of 540 kg, forward CG and MTOW of 620 kg, and at mid CG. The analysis results satisfy CS-VLA 181 from the stall speed to maximum speed.

The Phugoid and short mode responses are presented in Figure 16(a) and (b) for the cruise condition,

respectively. The four basic responses of the longitudinal dynamic characteristics are observed after a small disturbance. Most of the responses in Phugoid mode are damped and disappear after three cycles, as shown in Figure 16(a). The short mode responses are heavily damped with small disturbance, as shown in Figure 16(b).

Lateral motions

Static lateral characteristics. The static lateral derivatives requirements are recommended for this light aircraft, as shown in Table 7.[27,32,33] The analysis results of the CDR stage satisfy CS-VLA177 under the mid CG condition. The results of the PDR stage show lateral static stability, but it was marginal at the PDR stage. It was recommended to extend the chord and span of the ventral fin to increase the vertical tail area. This results in the increase of $C_{n\beta}$ at the CDR stage.

The mapping static yawing and rolling derivatives with similar speed regime aircrafts are shown in Figure 17(a) and (b).[25] The VLA_CDR of $C_{n\beta}$ moves a little bit higher compared to VLA_PDR due to the increase of the ventral fin in the CDR configuration. The $C_{l\beta}$ coefficient shows a relatively close value to similar speed regime aircrafts in Figure 17(b). Thus, the VLA_CDR lateral static characteristics satisfy the CS_VLA 177 regulation for static lateral stability.[28]

Dynamic lateral characteristics. The lateral derivative coefficients, corrected at a cruise speed of 60 m/s from the wind tunnel test data, are presented in Table 8. Comparison with results from the PDR stage is shown for the lateral derivative coefficients. The lateral derivative coefficients from the AVL results have a similar trend compared to the wind tunnel test data at the corrected speed. However, the control effectiveness of

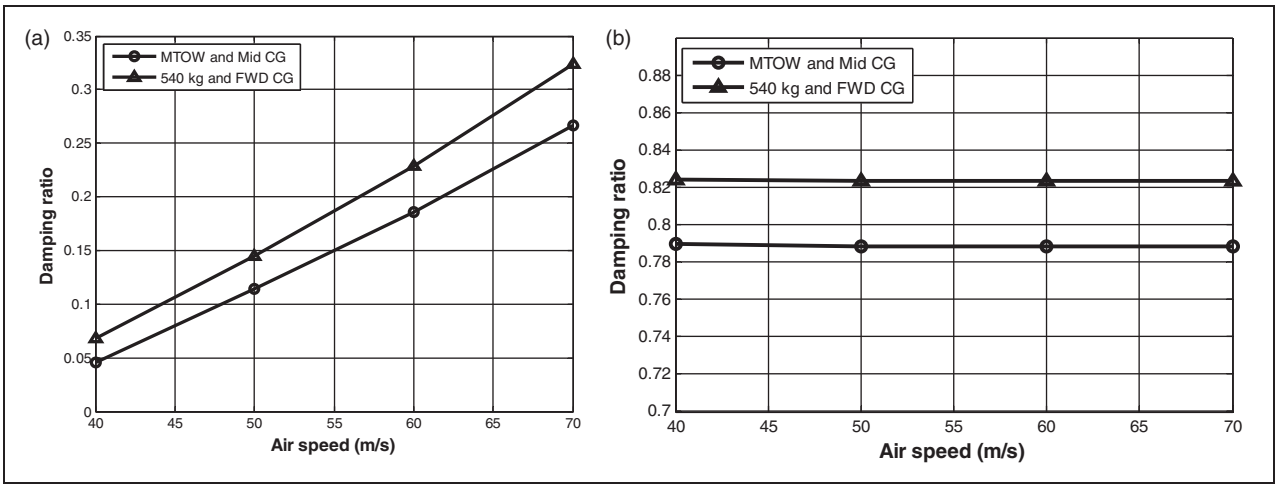

Figure 15. Longitudinal dynamic characteristics: (a) Phugoid mode damping ratio; (b) short mode damping ratio.

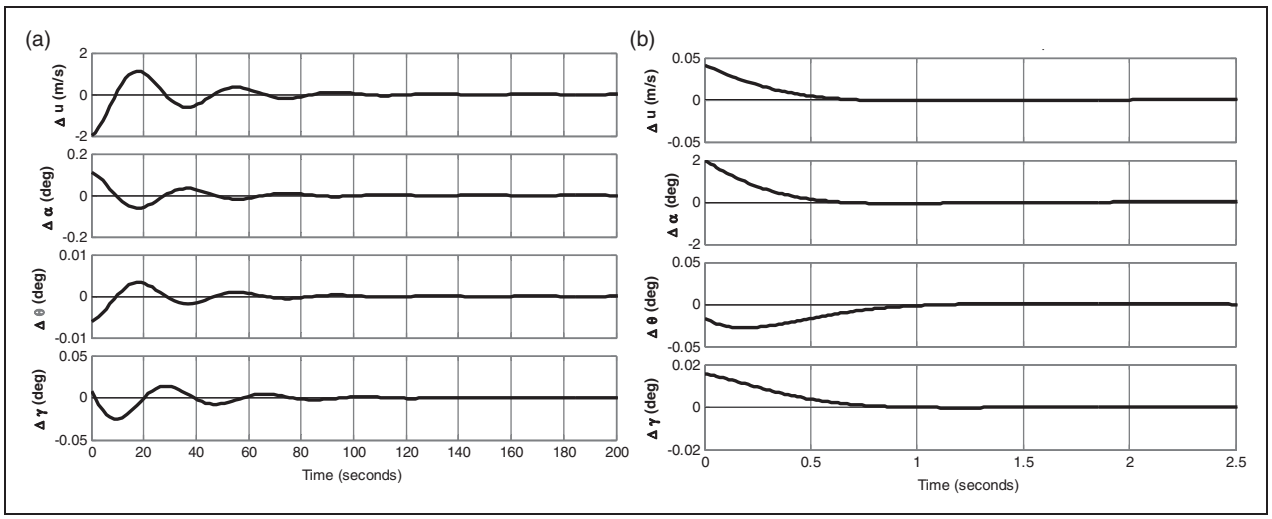

Figure 16. Longitudinal dynamic stability of light aircraft: (a) Phugoid mode response; (b) short mode response.

the rudder and aileron including $C_{l\delta a}$ and $C_{n\delta r}$ shows poor prediction results compared to the wind tunnel test data, as shown in Table 8 due to the limitations of the linear panel analysis code – AVL used at the earlier design stage.[13] The panel code – AVL has poor prediction results for the non-linear regions such as high AoA and control surface deflections. It results in the poor prediction for the lateral and directional control effectiveness as shown in Table 8.

The corrected lateral derivatives from the wind tunnel test are used to analyze the lateral dynamic characteristics of the light aircraft to enhance the results at the CDR stage compared to results at the PDR results and comply with CS-VLA 181.

The lateral motion equation is equation (6), where $x = [\Delta v, \Delta p, \Delta r, \Delta\phi]$ is the state vector, $\eta = [\Delta\delta_a, \Delta\delta_r]$ is the control vector, and matrices A and B contain the stability and control derivatives, as shown in Table 8.[34] The CS-VLA 181 regulation requirements indicate that the number of cycles in Dutch-roll mode amplitude must be reduced to 1/10 of the initial amplitude within seven cycles, as shown in Table 9. The handling qualities requirements of light aircraft for Dutch-roll, spiral, and roll mode are presented in Table 9 to compare with the analysis results at the PDR and CDR stage.[32,33] The solutions of lateral governing equation (6) with the lateral derivatives in Table 8 are shown in Table 9. The detailed MOI results at the CDR stage are also used to determine the lateral dynamic characteristics. The results at the PDR stage show more positive prediction results compared to the results at the CDR stage for most cases. The VLA_PDR results are heavily damped in the Dutch-roll mode within two cycles to reduce the amplitude to 1/10 of the initial amplitude. The damping factor in Dutch-roll mode ζ_{DR} shows the satisfaction of the handling qualities requirements; however, the PDR results are almost twice the CDR results. Moreover, the natural frequency of the Dutch-roll shows satisfaction of the handling qualities requirements. The PDR prediction results show the right trend for the prediction of lateral dynamic characteristics.

The Dutch-roll responses are presented in Figure 18(a) at a cruise speed of 60 m/s with the lateral derivatives corrected. The response oscillation disappears after the maximum four cycles in Figure 18(a) at the cruise speed for the four lateral responses. The number of cycles to halve the amplitude in Dutch-roll mode is shown, from 20 m/s to 70 m/s, in Figure 18(b). The number of cycles in Dutch-roll mode is heavily damped to halve the amplitude within less than 1 cycle. Therefore, it satisfies the CS-VLA 181 regulation requirement from the stall speed to maximum speed.

Table 7. Lateral motion: Static characteristic and CS-VLA 177 compliance checking.

Requirements	VLA_CDR	VLA_PDR	Evaluation	Note
$C_{l\beta}(1/\text{rad}) < 0$	−0.175	−0.083	Satisfied	Mid CG
$0.05 < C_{n\beta}(1/\text{rad}) < 0.4$	0.075	0.049	Satisfied	Mid CG

Conclusion

The stability and control analysis using the wind tunnel test data process is proposed and developed

Table 8. Lateral derivatives comparison.

Derivatives	VLA_CDR (W/T data)	VLA_PDR (AVL data)	Note
$C_{y\beta}$	−0.541	−0.446	1/rad
$C_{n\beta}$	0.075	0.109	1/rad
$C_{l\beta}$	−0.175	−0.137	1/rad
C_{yp}	0	−0.228	1/rad
C_{np}	−0.04	−0.0034	1/rad
C_{lp}	−0.8573	−0.566	1/rad
C_{yr}	0.2647	0.278	1/rad
C_{nr}	−0.0642	−0.114	1/rad
C_{lr}	0.0915	0.0817	1/rad
$C_{n\delta a}$	−0.0156	−0.0016	1/rad
$C_{l\delta a}$	0.1356	0.1032	1/rad
$C_{n\delta r}$	−0.0471	−0.0459	1/rad
$C_{l\delta r}$	0.0096	0.0072	1/rad

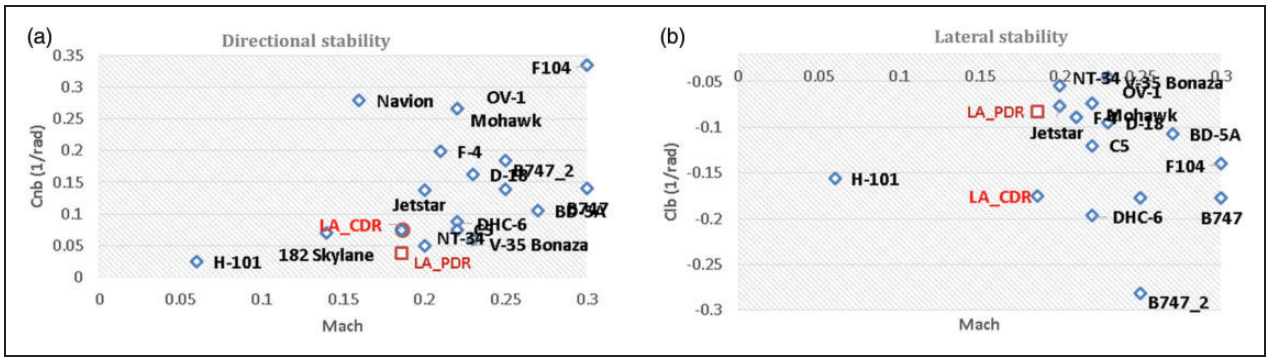

Figure 17. Static lateral characteristics of LA comparison: (a) yawing static stability derivative; (b) rolling static stability derivative.

Table 9. Lateral motion characteristic and CS-VLA 181 compliance check.

Requirements	VLA_CDR	VLA_PDR	Evaluation	Note
N_{DR} *1/10* amplitude in 7 cycles	~4	~2	Satisfied/Reg	$V_{min} \sim V_{max}$
$\zeta_{DR} \geqslant 0.08$	0.1581	0.25	Satisfied	Cruise speed
Roll time constant: $T_{1/2} < 1.4$ (s)	0.486	*x*	Satisfied	Cruise speed
Spiral mode: $T_{1/2} > 20$ (s)	62.27	*x*	Satisfied	Cruise speed
$-1 \leqslant C_{nr} \leqslant -0.1$	−0.072	−0.114	Satisfied	Cruise speed
$\omega_{nDR} > 0.4$	2.934	4.32	Satisfied	Cruise speed
$\zeta_{DR} * \omega_{nDR} > 0.15$ (rad/s)	0.3520	1.08	Satisfied	Cruise speed

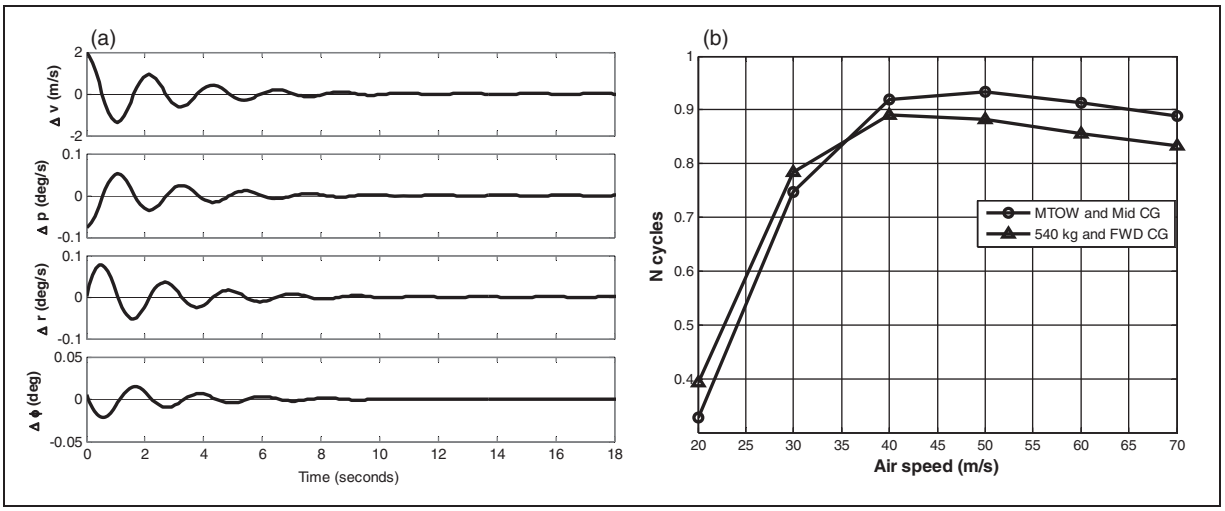

Figure 18. Lateral motion characteristics: (a) Dutch-roll response; (b) the number of cycles in Dutch-roll mode to halve the amplitude.

successfully and efficiently for a CS-VLA certified aircraft at the PDR and CDR stages. The aerodynamic characteristics of a 20% scale wind tunnel test model are investigated and provided for the longitudinal and lateral aerodynamics with flap, elevator, rudder, and aileron deflections. The winglet effect test results are also provided and discussed. Correction of the Mach and Reynolds numbers from the 20% test scale model is made for the stability and control analysis at a later step to provide more reliable analysis results.

The comprehensive aerodynamic characteristics of a new light aircraft from the wind tunnel test data are presented and investigated for the longitudinal and lateral aerodynamic coefficients. The main effects of control surfaces including elevator, aileron, rudder, and flap on the main aerodynamic coefficients show the correct behaviors and responses to the control surface deflections. The flap effects show the proper increment in lift when deflecting for the takeoff and landing condition. In addition, the winglet effect results show the better aerodynamic performance of lift-to-drag ratio at the cruise condition.

The stability and control analysis results of the longitudinal and lateral motions are investigated and compared with the previous PDR analysis results to enhance the PDR and CDR analysis results in the aircraft design development process. The CDR stability and control analysis results, using the most reliable aerodynamics from the wind tunnel test with corrected Mach and Reynolds numbers, accurate MOI, and CG envelope from the detailed mass breakdown, are compliant with CS-VLA 173, CS-VLA 177, and CS-VLA 181. Compliance with these regulations is observed from the CDR analysis results. The trend of PDR aerodynamic inputs and analysis results also shows agreement with the CDR analysis results. It concluded that the CS-VLA certified aircraft configuration is fixed after the CDR stage.

Declaration of conflicting interests

The author(s) declared no potential conflicts of interest with respect to the research, authorship, and/or publication of this article.

Funding

The author(s) disclosed receipt of the following financial support for the research, authorship, and/or publication of this article: This paper was supported by Konkuk University in 2014.

References

1. General Aviation Manufacturers Association (GAMA) report, http://www.bga-aeroweb.com/General-Aviation.html#Q (accessed 30 November 2015).
2. Van Nguyen N, Neufeld D, Kim S, et al. Multidisciplinary configuration design optimization for advanced very light aircraft. In: *The Korean Society for Aeronautical & Space Sciences (KSAS) conference*, Cheju Island, Korea, 2011, pp.18–23.
3. Nicolosi F, de Marco A and Della Vecchia P. Flight tests, performances, and flight certification of a twin-engine light aircraft. *J Aircraft* 2011; 48: 177–192.
4. Biber K. Stability and control characteristics of a new FAR 23 Airplane. *J Aircraft* 2006; 43: 2006.
5. Nicolosi F, de Marco A and Della Vecchia P. Stability, flying qualities and longitudinal parameter estimation of a twin-engine CS-23 certified light aircraft. *Aerosp Sci Technol* 2013; 24: 226–240.
6. Cummings RM and Schütte A. Integrated computational/experimental approach to unmanned combat air vehicle stability and control estimation. *J Aircraft* 2012; 49: 1542–1557.
7. Anton N, Botez RM and Popescu D. Stability derivatives for a delta-wing X-31 aircraft validated using wind tunnel test data. *Proc IMechE, Part G: J Aerospace Engineering* 2010; 225.
8. Lee J and Yoon S. Estimation and validation of lateral-directional stability/control derivatives for the Flight Training Device of a light aircraft. *Simulat Model Pract Theory* 2008; 16: 1–14.
9. Pettersson K and Rizzi A. Aerodynamic scaling to free flight conditions: Past and present. *Prog Aerosp Sci* 2008; 44: 295–313.
10. Traub LW. Drag extrapolation to higher Reynolds number. *J Aircraft* 2009; 46.
11. Thamarai Selvi S, Mahendran E and Rama S. Neural network-based interpolation and extrapolation of wind tunnel test data. *Int J Comput Intell Appl* 2009; 8: 225–235.
12. Owens LR, Wahls RA, Elzey MB, et al. Reynolds number effects on off-design stability and control characteristics of supersonic transports. *J Aircraft* 2007; 44.
13. Vortex-Lattice Method (AVL 3.35), http://web.mit.edu/drela/Public/web/avl/ (accessed 30 November 2015).
14. Neufeld D, Van Nguyen N, Kim S, et al. A multidisciplinary possibilistic approach to light aircraft conceptual design. In: *53rd AIAA/ASME/ASCE/AHS/ASC structures, structural dynamics and materials conference*, Honolulu, Hawaii, AIAA 2012-1434, 2012.
15. Blake WB. The USAF stability and control digital DATCOM. Volume I, User Manual, Airforce Flight Dynamics Laboratory, AFFDL-79-3032, April 1979.
16. Van Nguyen N, Lee D, Park H-U, et al. A multidisciplinary robust optimization framework for UAV conceptual design. *Aeronaut J* 2014; 118: 123–142.
17. Van Nguyen N, Tyan M, Kim S, et al. Possibility-based multidisciplinary optimisation for electric-powered unmanned aerial vehicle design. *Aeronaut J* 2015; 119.
18. Stability and Control Analysis Report, Critical Design Review (CDR) Report, Konkuk University, June 2015.
19. Light Aircraft Development – V204 Experiment Test Report, Republic of Korea Air Force Academy, 27 November 2014.
20. KLA-100 Aircraft Specification, SH 0100 0001_04, Flight Design Gmbh, 7 July 2014.
21. Flight Design, "CTSW", http://flightdesign.com/wordpress/?page_id=39 (accessed 30 November 2015).
22. Park J, Tyan M, van Nguyen N, et al. Flap design optimization for KLA-100 aircraft in compliance with airworthiness certification. *Int J Korean Soc Aeronaut Space Sci* 2013; 41: 649–656.
23. Kaushik B and Anemaat WAJ. Methods to scale subsonic wind tunnel data to full-scale. In: *30th AIAA applied aerodynamics conference*, New Orleans, LA, USA, AIAA 2012-3228, 25–28 June 2012.
24. Yamauchi GK and Johnson W. Trends of Reynolds number effects on TWQ - Dimensional airfoil characteristics for helicopter rotor analyses, NASA-Ttl-b4363, April 1983.
25. Gudmundsson S. *General aviation aircraft design: Applied methods and procedures*. 1st ed. Oxford, UK; Waltham, MA: Butterworth-Heinemann, 2014.
26. Light aircraft stability and control analysis report for PDR, Konkuk University, 2014.
27. Sadraey MH. *Aircraft design: A systems engineering approach*. 1st ed. New York: John Wiley & Sons, Ltd, 2013.
28. Certification Specifications for Very Light Aeroplanes CS-VLA, European Aviation Safety Agency, 5 March 2009.
29. Nelson R. *Flight stability and automatic control*. 2nd ed. New York: McGraw Hill, 1997.
30. Etkin B and Reid LD. *Dynamics of flight: Stability and control*. 3rd ed. New Delhi: Wiley India Pvt Ltd, 2010.
31. Dommasch DO, Sherby SS and Connolly TF. *Airplane aerodynamics*. 4th ed. London: Pitman Publishing, 1967.
32. Anonymous. Flying qualities of piloted airplanes, MIL-F-1797C, Air Force Flight Dynamic Laboratory WPAFB, Dayton, USA, 1990.
33. Anonymous. Military Specification Flying Qualities of Piloted Airplanes, MIL-F-8785C, Air Force Flight Dynamic Laboratory WPAFB, Dayton, USA, 1980.
34. Stengel RF. *Flight dynamics*. Princeton, NJ: Princeton University Press, 2004.

Appendix

Notation

C_D	drag force coefficient
C_L	lift force coefficient
C_y	side force coefficient
C_m	pitching moment coefficient
C_n	yawing moment coefficient
C_l	rolling moment coefficient
C_{D_u}	drag coefficient with forward speed
C_{D_0}	zero-lift drag coefficient
C_{L_0}	zero angle-of-attack lift coefficient
C_{L_u}	lift coefficient with forward speed
C_{L_a}	lift curve slope
$C_{Z_{\dot{a}}}$	downwash lag on lift and tail
C_{Z_q}	effect of pitch rate on lift
$C_{Z_{\delta_e}}$	effect of elevator deflection on lift

C_{m_u}	effect of thrust, slipstream, and flexibility
C_{m_a}	static longitudinal stability
$C_{m_{\dot{a}}}$	downwash lag on moment
C_{m_q}	damping in pitch
$C_{m_{\delta_e}}$	elevator deflection in pitch
C_{l_β}	coefficient of rolling moment due to sideslip
$C_{n\beta}$	coefficient of yawing moment due to sideslip
$C_{y\beta}$	coefficient of lateral force due to sideslip
C_{l_p}	coefficient of rolling moment due to roll rate
C_{n_p}	coefficient of yawing moment due to roll rate
C_{y_p}	coefficient of lateral force due to roll rate
C_{l_r}	coefficient of rolling moment due to yaw rate
C_{n_r}	coefficient of yawing moment due to yaw rate
C_{y_r}	coefficient of lateral force due to yaw rate
$C_{y\delta_a}$	coefficient of lateral force due to aileron deflection
$C_{y\delta_r}$	coefficient of lateral force due to rudder deflection
$C_{n\delta_a}$	coefficient of yawing moment due to aileron
$C_{n\delta_r}$	coefficient of yawing moment due to rudder
$C_{l\delta_a}$	coefficient of rolling moment due to aileron
$C_{l\delta_r}$	coefficient of rolling moment due to rudder
I_{xx}	moment of inertia about x-axis (kg.m^2)
I_{yy}	moment of inertia about y-axis (kg.m^2)
I_{zz}	moment of inertia about z-axis (kg.m^2)
I_{xy}	product of inertia in the xy-planes (kg.m^2)
I_{xz}	product of inertia in the xz-planes (kg·m^2)
I_{yz}	product of inertia in the yz-planes (kg·m^2)
M	Mach number
N_{DR}	number of cycles in Dutch-roll
Re	Reynolds number
$T_{1/2}$	time to halving the amplitude (s)
ΔC_{Lmax}	increment in lift coefficient
Δp	disturbance in rolling rate (deg/s)
Δu	disturbance in forward speed (m/s)
$\Delta\alpha$	disturbance in AoA (deg)
$\Delta\alpha_{max}$	increment in angle of attack (deg)
$\Delta\delta_a$	aileron control (deg)
$\Delta\delta_e$	elevator control (deg)
$\Delta\delta_r$	rudder control (deg)
$\Delta\delta_T$	propulsive control
$\Delta\gamma$	disturbance in flight path angle (deg)
$\Delta\nu$	disturbance in sideslip speed (m/s)
$\Delta\phi$	disturbance in bank angle (deg)
Δr	disturbance in yawing rate (deg/s)
$\Delta\theta$	disturbance in pitch angle (deg)
ω_n	natural frequency (rad/s)
ξ	damping ratio

Subscripts

DR	Dutch-roll mode
$M@WT$	Mach number at wind tunnel test condition
$M@flight$	Mach number at flight condition
$Phugoid$	Phugoid motion mode
$Short$	short motion mode